CT vs. MRI in nasal cavity modeling: implications for CFD simulations and model consistency

Filip Trnka [1*], *Hana* Schmirlerová[1], *Marie* Raušová[1], *David* Netuka[2], and *Martin* Májovský[2]

[1] CTU in Prague, Faculty of Mechanical Engineering, Department of Fluid Dynamics and Thermodynamics, Technická 4, 160 00 Prague, Czech Republic
[2] Charles University and Military University Hospital, First Faculty of Medicine, Department of Neurosurgery and Neurooncology, U Vojenské nemocnice 1200, 169 02 Prague 6, Czech Republic

Abstract. The use of computed tomography (CT) and magnetic resonance imaging (MRI) in medicine has significantly increased over the past decade, enabling the creation of accurate patient-specific anatomical models. This study aims to compare CT and MRI scans in the reconstruction of nasal cavity geometries and their subsequent impact on computational fluid dynamics (CFD) simulations. Patient-specific models were generated from both CT and MRI datasets using 3D Slicer, and airflow simulations were performed in ANSYS Fluent. The resulting models exhibited substantial geometric differences: CT-based models showed approximately four times higher volume intensity range compared to MRI-based models. Additionally, the segmentation and model preparation from MRI data required 16 hours longer than for CT data of the same patient. These findings indicate that models derived from CT and MRI scans are not directly interchangeable for CFD analysis of nasal airflow. Consequently, combining CT- and MRI-based datasets within a single study may lead to inconsistencies in simulation results.

1 Introduction

In recent years, medical imaging methods have been increasingly used for computational fluid dynamics (CFD) simulations [1], [2], [3]. Many authors employ patient-specific geometries of organs such as the heart, blood vessels, or airways, reconstructed from clinical imaging modalities including computed tomography (CT), magnetic resonance imaging (MRI), for two- or three-dimensional visualization [4], [5], [6], [7], [8], [9].

Both CT and MRI provide volumetric data stored as a series of two-dimensional grayscale images in the DICOM format. To reconstruct a three-dimensional model, specialized software is used to segment the region of interest from each image slice and connect it to the corresponding regions in adjacent slices. This process results in a continuous 3D object that accurately represents the anatomical structure. The chosen imaging modality and the quality of the segmentation process are therefore crucial factors influencing the final geometry used in CFD simulations [8].

CT utilizes X-ray radiation to capture high-resolution images with excellent contrast between air, bone, and soft tissue, making it particularly suitable for modelling airways and skeletal structures [10], [11]. MRI, in contrast, employs a strong magnetic field and radiofrequency pulses to obtain images without ionizing radiation, offering better soft tissue contrast but typically lower spatial resolution and longer acquisition times [11], [12].

This study presents a comparison of CFD results based on nasal cavity models reconstructed from CT and MRI scans of the same patient. The aim is to evaluate the consistency and suitability of both imaging modalities for CFD analysis and to assess whether data from CT and MRI can be interchangeably used or combined in larger cohort studies.

2 Methods

2.1 Creating models from CT and MRI scans

CT and MRI datasets of the same patient were obtained from clinical imaging records in DICOM format. The data were imported into 3D Slicer, where segmentation of the nasal cavity was performed using a combination of thresholding, region-growing, and manual correction tools. The detailed segmentation procedure follows the methodology described in [8], where identical techniques were applied to CT data from a different patient.

In contrast, MRI scans required extensive manual refinement due to the lower contrast between air and soft tissue in the nasal region. The segmentation of the MRI-based model required approximately 16 additional hours compared to the CT dataset used in this study. The volume intensity range for the CT scans was approximately 45,000 points, whereas the MRI scans exhibited a range of only about 9,500 points.

* Corresponding author: f.trnka@fs.cvut.cz

In both cases, patients were in good physical and physiological condition prior to scanning. For both models, the secondary sinuses were excluded to reduce computational time, and their coordinate systems were aligned to ensure geometric consistency.

The resulting surface models were exported in STL format and smoothed to remove artifacts while preserving anatomical fidelity. Each model represented the complete nasal passage—from the nostrils to the nasopharynx—excluding the secondary sinuses and was subsequently prepared for meshing and CFD analysis.

2.2 Meshing

The computational meshes were generated in ANSYS Meshing using an unstructured polyhedral grid with prism layers near the walls to accurately capture boundary layer effects. The same meshing parameters were applied to both models to ensure consistency, following the mesh independence study described in Section 2.3. The CT-derived model contained approximately 5.5 million elements, while the MRI-based model consisted of a similar number, differing by only about 50,000 cells. Special care was taken to maintain high mesh quality, with skewness values kept below 0.8 for both cases.

2.3 Mesh independence

To verify that the simulation results were independent of mesh resolution, a mesh independence study was conducted as part of a diploma thesis by one of the co-authors [13]. The study involved generating and comparing 30 volume meshes to ensure numerical stability while maintaining a reasonable computational cost. The total number of cells ranged from approximately 0.7 million to 16 million.

The main criterion for mesh selection was based on the differences in pressure and velocity between subsequent refinements, which were both below 2% at the nostril and nasopharyngeal planes for the selected mesh. Based on the evaluation of flow parameters and computational efficiency, the mesh containing 6.4 million elements was identified as optimal, providing the best balance between accuracy and runtime.

The selected mesh was characterized by a minimum cell size of 0.25 mm and a maximum cell size of 0.5 mm, with a surface normal angle of 18°. The polyhedral volume mesh included six prism layers near the walls, with a last aspect ratio of 2.23 and a maximum cell size of 0.6 mm in the volume region.

2.4 Boundary Condition

Boundary conditions were defined to represent steady inspiratory airflow within the nasal cavity, following the approach described in [1]. The nostrils were modelled as pressure inlets with zero-gauge pressure, while the outlet, located downstream of the nasopharynx, was defined as a mass-flow outlet, consistent with the setup described in [8]. The nasal walls were assumed to be rigid and stationary, with no-slip boundary conditions applied. Air was modelled as an incompressible, Newtonian fluid with constant density and viscosity under standard ambient conditions.

The present model does not account for humidification of inspired air. While water vapor slightly alters air density and viscosity, its impact on nasal airflow velocities under resting or moderate breathing conditions is considered minor compared to the dominant influence of nasal geometry. Moreover, the analysis focuses on relative differences within the same patient derived from different imaging sources, for which such second-order property variations are unlikely to affect the comparative conclusions.

2.5 Solution

All CFD simulations were performed in ANSYS Fluent 2024 R2. The nasal cavity represents a highly complex geometry characterized by narrow, curved passages and varying cross-sectional areas. To accurately capture the airflow behaviour under these conditions, the realizable k–ε turbulence model was selected. This model offers improved performance for flows involving strong curvature, which are typical features of nasal airflow [14].

2.6 Post processing

Post-processing was carried out in ANSYS Fluent, focusing on the evaluation of velocity distribution, pressure drop, and airflow patterns within the nasal cavity to compare the results obtained from both models.

For model comparison, cross-sectional planes were created along the nasal passage based on the maximum distance between the nostrils (0%) and the nasopharynx (100%). Planes were positioned at 35%, 55%, and 75% of the total passage length measured from the anterior (nostril) end. Figure 1 illustrates the location of the planes in the CT and MRI based models.

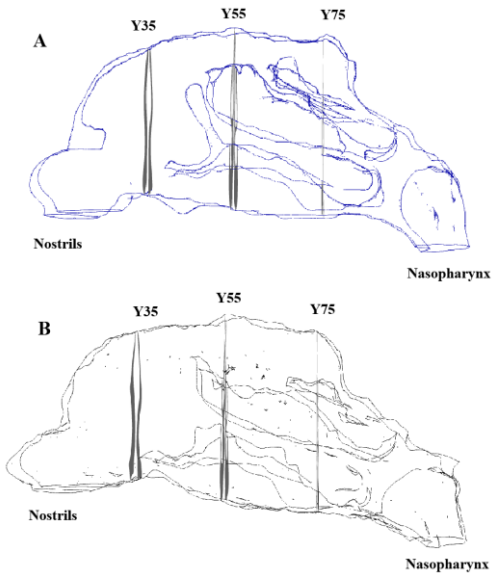

Figure 1. *A* – Cross section planes in CT model and *B* - Cross section planes in MRI model for displaying results.

3 Results and Discussion

The procedures for creating CT- and MRI-based models were identical, and the coordinate systems of both models were aligned using the 3D Slicer software. However, despite following the same methodology, notable differences occurred during model generation. The most significant difference was the time required for segmentation of the MRI model. It required approximately 16 additional hours of work compared to the CT model.

Another major difference was observed in the total model volume. The CT-derived model had a volume of 29,63 mL, while the MRI-derived model measured 25,76 mL, corresponding to a difference of 13%. These volumetric discrepancies are illustrated in Figure 2.

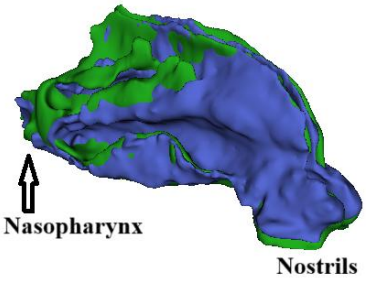

Figure 2. Comparison of CT model (green) and MRI model (blue).

Despite the higher total volume of the CT-derived model, the most apparent geometric differences were observed in the cross-sectional regions. For example, the MRI model showed narrower upper meatus passages compared to the CT model, while the middle meatus appeared slightly wider in the MRI geometry.

Figure 3 presents the velocity field distributions on coronal planes for both models. The evaluation of all analysed cross-sectional planes revealed not only differences in the total cross-sectional area but also in the overall geometry, particularly in the upper and lower meatus of the nasal cavity. In the middle meatus, where volumetric airflow is concentrated, the geometric differences between the CT- and MRI-derived models were less pronounced, likely due to the smaller presence of soft tissue and the dominant influence of the bony nasal conchae in this region.

Plane Y35 is located closest to the nasal entrance. Even here, a noticeable geometric discrepancy between the models was observed. In the MRI-derived model, the cavities in both the upper and lower meatus appeared significantly different from those in the CT-derived model. These geometric variations directly influenced the velocity field distribution observed in the CFD simulations.

Distinct geometric differences were again visible across the entire cross-sectional area of Plane Y55. The MRI-derived model showed a considerably smaller area between the middle concha and the lateral wall of the nasal cavity, and a “wavier” shape of the lower projections compared to the CT model. Variations in velocity distribution—while neglecting the absolute mean velocity difference—were most evident in the lower portion of the cavity. In the MRI model, the flow tended to remain closer to the medial wall, whereas in the CT model, it deviated more laterally. However, since this observation is based on velocity magnitude contours, the exact directionality of flow would require further verification. Overall, the main airflow stream showed comparable distribution between both models, with more pronounced differences occurring primarily in the peripheral regions.

Plane Y75 exhibited the most significant geometric variation in the upper meatus of the nasal cavity, where the conchoidal structures changed their shape and orientation entirely. As a result, the comparison of velocity fields in these upper peripheral areas lost interpretative value. Nevertheless, in the middle and lower meatus of the cross-section, the flow field remained more comparable, corresponding to the generally similar geometry of these regions.

In addition to the velocity field analysis, pressure distribution along the nasal cavity was also evaluated. The static pressure between the nostrils (inlet) and the nasopharynx plane decreased by 20.77 Pa in the CT-derived model and by 31.11 Pa in the MRI-derived model. A similar trend was observed in the total pressure drop, with values of 17 Pa for the CT model and 26.24 Pa for the MRI model. Although the MRI model exhibits a slightly wider middle meatus, its overall narrower geometry, particularly in the upper and lower regions of the cavity, leads to greater overall flow resistance and consequently higher pressure loss compared to the CT-based model.

If the objective of a CFD study were limited to tracking the main airflow stream, such as in investigations of inhaled drug transport or airflow distribution toward the lungs, these geometric discrepancies between CT- and MRI-based models would likely have a negligible impact on overall conclusions.

However, if the study focuses on more localized phenomena, such as wall shear stress in the olfactory region or detailed airflow–surface interactions, maintaining the true anatomical geometry becomes critical. Therefore, when comparing multiple cases or patients, it is essential to use a single imaging modality for model generation to ensure consistency and reliability of the results.

4 Conclusion

The comparison between CT- and MRI-derived nasal cavity models highlights both the potential and limitations of each imaging modality for CFD applications. CT scans provide superior geometric fidelity and segmentation efficiency due to their high spatial resolution and clear tissue–air contrast. However, they involve exposure to ionizing radiation, which may restrict their use in repeated clinical imaging. Conversely, MRI offers safer, radiation-free imaging but requires substantially more processing time and introduces uncertainties in surface definition.

ID	CT model	MRI model
Y35	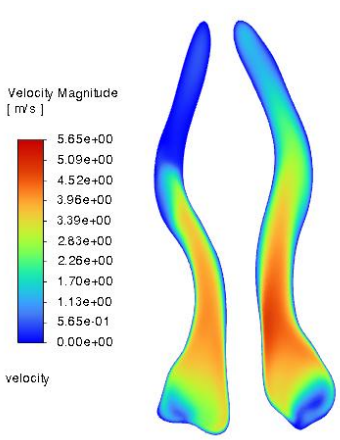	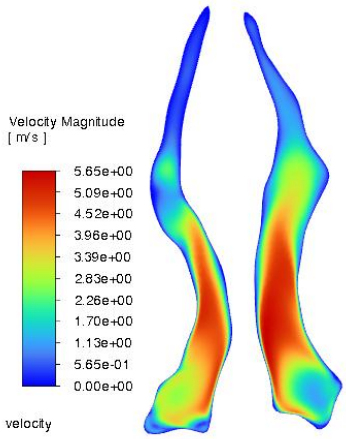
Y55	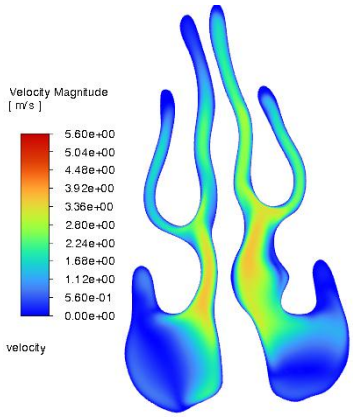	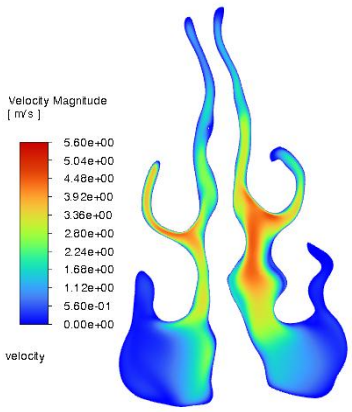
Y75	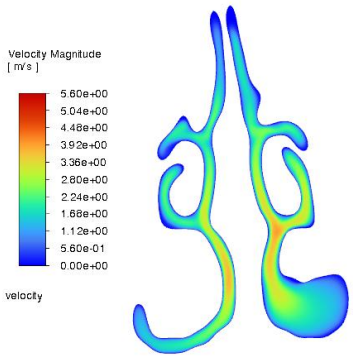	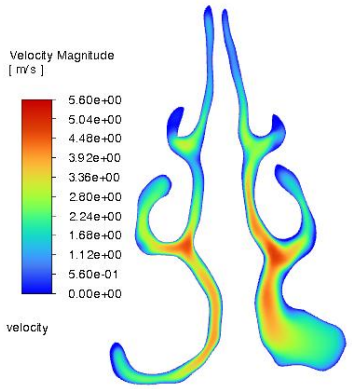

Figure 3. CFD results of velocity flow field in cross section planes in both models.

The observed differences in airflow resistance and geometric resolution indicate that CT- and MRI-based models cannot be directly combined within a single CFD study without introducing bias. For studies involving larger patient cohorts, it is therefore recommended to use a single imaging modality to ensure consistency and comparability of results.

Acknowledgments

This work was supported by the Grant Agency of the Czech Technical University in Prague, under Grant No. SGS25/128/OHK2/3T/12; Ministry of Defence of the Czech Republic under Grant No. MO1012; Ministry of Health of the Czech Republic under Grant No. NW24-08-00324; and Cooperation Neuroscience Charles University.

References

[1] R. Mösges, Computational fluid dynamics of the nasal cavity, in Nasal Physiology and Pathophysiology of Nasal Disorders, (Springer-Verlag Berlin Heidelberg, pp. 247–255. 2013), doi:10.1007/978-3-642-37250-6_19.

[2] K. Zhao, P. Malhotra, D. Rosen, P. Dalton, and E. A. Pribitkin, Computational Fluid Dynamics as Surgical Planning Tool: A Pilot Study on Middle Turbinate Resection. Anatomical Record, vol. **297**, no. 11, pp. 2187–2195, (Nov. 2014), https://doi.org/10.1002/ar.23033

[3] H. Salati, J. Bartley, and D. E. White, Computational Fluid Dynamics Simulation of Wall Shear Stress and Pressure Distribution from a Neti Pot During Nasal Saline Irrigation. J Med Biol Eng, vol. **41**, no. 2, pp. 175–184, (Apr. 2021), doi:10.1007/s40846-020-00589-6.

[4] M. Toğaçar, Z. Cömert, and B. Ergen, Classification of brain MRI using hyper column technique with convolutional neural network and feature selection method. Expert Syst Appl, vol. **149**, p. 113274, Jul. 2020, https://doi.org/10.1016/j.eswa.2020.113274

[5] G. G. Handsfield, C. H. Meyer, J. M. Hart, M. F. Abel, and S. S. Blemker, Relationships of 35 lower limb muscles to height and body mass quantified using MRI. J Biomech, vol. **47**, no. 3, pp. 631–638, (Feb. 2014), https://doi.org/10.1016/j.jbiomech.2013.12.002.

[6] Y. Liu, M. R. Johnson, E. A. Matida, S. Kherani, and J. Marsan, Creation of a standardized geometry of the human nasal cavity. J Appl Physiol, vol. **106**, p. 59, (2009), https://doi.org/10.1152/japplphysiol.90376.2008

[7] D. Zwicker, K. Yang, S. Melchionna, M. P. Brenner, B. Liu, and R. W. Lindsay, Validated reconstructions of geometries of nasal cavities from CT scans. Biomed Phys Eng Express, vol. **4**, no. 4, (Jun. 2018), doi:10.1088/2057-1976/aac6af.

[8] F. Trnka, H. Schmirlerová, M. Májovský, D. Netuka, and M. Schmirler, Preparation of a Real Model of Nasal Cavities from Computed Tomography for Numerical Simulation. MATEC Web of Conferences, vol. **369**, p. 01005, (2022), https://doi.org/10.1051/matecconf/202236901005

[9] F. Trnka, H. Schmirlerová, M. Májovský, D. Netuka, and M. Schmirler, Examining the Impact of Inlet Shape on Nasal Cavity Flow Field: A Computational Investigation. MATEC Web of Conferences, vol. **383**, p. 00021, (Oct. 2023), doi: 10.1051/matecconf/202338300021.

[10] E. Seeram, Computed Tomography: Physical Principles and Recent Technical Advances. J Med Imaging Radiat Sci, vol. **41**, no. 2, pp. 87–109, (Jun. 2010), https://doi.org/10.1016/j.jmir.2010.04.001

[11] A. E. M. Eltorai, C. H. Hyman, and T. T. Healey, How Does Magnetic Resonance Imaging Work? In: Essential Radiology Review. (Springer, Cham. 2019). https://doi.org/10.1007/978-3-030-26044-6_163

[12] Berger A. Magnetic resonance imaging. BMJ.324(7328):35 (Jan 2002). doi: 10.1136/bmj.324.7328.35

[13] M. Raušová, The Effect of Neglecting Transient Flow in Nasal Cavity CFD Simulations, Master Thesis. CTU in Prague, Prague 2025

[14] Trnka F, Schmirlerova H, Schmirler M, et al. Changes in Nasal Anatomy and Airflow After Endoscopic Resection of Pituitary Adenomas Using Computational Fluid Dynamics: A Pilot Study. Cureus (6): e85568, (June 08, 2025). doi:10.7759/cureus.85568